Liu et al. *Zool. Res.* 2026, 47(3): 748−764
https://doi.org/10.24272/j.issn.2095-8137.2025.499
https://cstr.cn/32248.14.zr.2025.499

ZR | Zoological Research

Article Open Access

First identification of an amphibian-derived peptide with anti-vascular aging activity

Xin Liu[1,#], Jie Liu[1,#], Bin Li[3,#], Zi-Han Qian[1], Guo-Rui Zhang[1], Hao-Yang Gan[1], Zhi-Ruo Li[1], Xiao-Ya Han[1], Zhuo Wang[1], Yuan-Sheng Li[1], Xin-Yan Zheng[1], Li-Tian Wang[1], Sai-Ge Yin[1], Wen-Rou Su[5], Li He[4,*], Ying Wang[2,*], Ming-Ying Luo[1,*], Xin-Wang Yang[1,*]

[1] *Key Laboratory of Skin and Mucosal Injury Repair*, *Regeneration* & *Active Peptides of Yunnan Provincial Department of Education*, *Regenerative Medicine Research Center*, *Faculty of Basic Medical Science*, *Kunming Medical University*, *Kunming*, *Yunnan* 650500, *China*

[2] *Key Laboratory of Chemistry in Ethnic Medicinal Resources*, *State Ethnic Affairs Commission* & *Ministry of Education*, *School of Ethnic Medicine*, *Yunnan Minzu University*, *Kunming*, *Yunnan* 650504, *China*

[3] *Department of Cardiac and Vascular Surgery*, *First Affiliated Hospital of Kunming Medical University*, *Kunming*, *Yunnan* 650500, *China*

[4] *Department of Dermatology*, *First Affiliated Hospital of Kunming Medical University*, *Kunming*, *Yunnan* 650032, *China*

[5] *Yunnan Yunke Characteristic Plant Extraction Laboratory Co.*, *Ltd.*, *Kunming*, *Yunnan* 650106, *China*

ABSTRACT

Vascular aging is a principal driver of cardiovascular morbidity and mortality, and effective prevention of age-related vascular pathologies depends on interventions that target fundamental molecular and cellular aging pathways. The present study investigated the anti-vascular aging activity of AL-VI10, a novel bioactive peptide derived from amphibian skin, together with the underlying mechanism. Notably, AL-VI10 exhibited excellent biosafety, with no detectable cytotoxic or hemolytic activity, and showed potent free radical scavenging capacity, enhanced antioxidant enzyme activity, and reduced reactive oxygen species (ROS) accumulation. In a D-galactose-induced mouse model of aging, AL-VI10 significantly attenuated vascular aging-associated phenotypes, including increased medial thickness, elevated expression of inflammatory cytokines, and up-regulation of matrix metalloproteinase levels, while simultaneously promoting autophagy. In hydrogen peroxide (H_2O_2)-induced senescent human umbilical vein endothelial cells, AL-VI10 reduced senescence-associated β-galactosidase (SA-β-gal) activity, down-regulated senescence markers p53 and p21, enhanced endothelial proliferation and migration, and increased endothelial nitric oxide synthase expression. Mechanistic analyses showed that AL-VI10 up-regulated silent information regulator 1 (SIRT1) and nuclear factor erythroid 2-related factor 2 (Nrf2). Pharmacological inhibition of SIRT1 suppressed AL-VI10-induced Nrf2 activation and weakened its anti-senescence effects, whereas inhibition of Nrf2 reversed ROS reduction and impaired endothelial recovery. Further analysis demonstrated direct binding of AL-VI10 to the extracellular domain of leukocyte differentiation antigen CD44 (CD44), and CD44 knockdown abolished activation of the SIRT1-Nrf2 axis and eliminated the anti-senescence activity of AL-VI10. These findings indicate that AL-VI10 alleviates vascular aging through CD44-dependent activation of SIRT1-Nrf2 signaling and identify amphibians as a promising source of bioactive compounds for anti-aging therapy.

Keywords: Peptides; Amphibians; Senescence; Aging; CD44-SIRT1-Nrf2 signaling pathway

INTRODUCTION

Vascular aging represents a defining feature of organismal senescence and a major determinant of cardiovascular decline and broader physiological deterioration. Increasing evidence identifies this process as a modifiable risk factor that strongly influences the initiation and progression of age-

Received: 14 December 2025; Accepted: 08 January 2026; Online: 09 January 2026

Foundation items: This work was supported by the First-Class Discipline Team of Skin & Mucosal Regenerative Medicine of Kunming Medical University (2024XKTDTS10), National Natural Science Foundation and of China (32301054, 32360138), Programs of Yunnan Fundamental Research Project (202301AS070036), Programs of Yunnan Applied Basic Research Project-Kunming Medical University Union Foundation (202301AY070001-301), Open Research Fund of Yunnan Characteristic Plant Extraction Laboratory (YKKF2024003) and High-level Health Technology Talent in Yunnan Province (L-2025003)

[#]Authors contributed equally to this work

*Corresponding authors, E-mail: drheli2662@126.com; wangying_814@163.com; luomingying0403@163.com; yangxinwang@kmmu.edu.cn

associated vascular dysfunction (Donato et al., 2018). This process is fundamentally driven by vascular endothelial cells, which preserve vascular homeostasis through coordinated regulation of angiogenesis, vasomotor function, and barrier integrity. Progressive accumulation of senescent endothelial cells disrupts these functions and drives a pathological program marked by reduced regenerative capacity, persistent oxidative stress, and a proinflammatory secretory phenotype. Together, these changes promote vascular stiffening, endothelial dysfunction, and systemic inflammation, all of which are recognized features of accelerated vascular aging and major predictors of cardiovascular morbidity (Augustin & Koh, 2024). Although substantial progress has been made in defining the molecular basis of endothelial senescence, effective translation of these advances into anti-aging therapies remains limited. This gap highlights the importance of identifying novel regulatory mechanisms and actionable molecular targets capable of attenuating or reversing vascular injury.

Bioactive peptides have emerged as an attractive therapeutic class due to their broad structural diversity, strong target selectivity, and favorable biocompatibility (Deng et al., 2026; Fu et al., 2026; Zhu et al., 2025). Their translational relevance is reflected in a rapidly expanding pharmaceutical development landscape, with multiple peptide-based therapeutics achieving regulatory approval and broad clinical application across diverse diseases (De La Torre & Albericio, 2020; Jia et al., 2024; Li et al., 2025b; Sun et al., 2023; Wei et al., 2025; Wu et al., 2024). Among these molecules, amphibian-derived peptides represent a particularly rich yet insufficiently explored reservoir of bioactive compounds, several of which have shown pronounced efficacy in vascular disorders associated with ischemic injury. For instance, the peptide OM-LV20 has been shown to enhance arteriogenesis through regulation of the miR-29b-3p/vascular endothelial growth factor A (VEGFA) axis, highlighting the dual potential of such peptides as both therapeutic agents and molecular probes for elucidating angiogenic regulatory pathways (Zhang et al., 2024b). Despite growing evidence of their antioxidant and anti-inflammatory properties, the application of amphibian-derived peptides to vascular aging remains largely unexplored. Given that oxidative stress is a major driver of endothelial senescence and vascular degeneration (Lu et al., 2024), amphibian peptides with redox-modulating capacity may provide a new strategy for intervention in age-related vascular dysfunction. Systematic investigation into their mechanisms of action may thus uncover previously unrecognized molecular targets and contribute to the development of next-generation vascular therapeutics.

Accumulating evidence indicates that senescent endothelial cells undergo extensive phenotypic reprogramming, driven by dysregulation of conserved longevity-associated pathways, including sirtuin, Nrf2, and mammalian target of rapamycin (mTOR) signaling (Shen et al., 2023). Within this regulatory network, silent information regulator 1 (SIRT1), a nicotinamide adenine dinucleotide (NAD^+)-dependent deacetylase, serves as a pivotal regulator of vascular homeostasis. Through coordinated regulation of redox balance, antioxidant defense, inflammatory signaling, and endothelial integrity, SIRT1 constrains vascular injury in part through crosstalk with downstream effectors such as Nrf2 (Tao et al., 2023). The SIRT1-Nrf2 axis has been implicated in multiple cardiovascular pathologies, and increasing evidence supports a protective role in the attenuation of diabetic endothelial dysfunction and ischemia-reperfusion-induced myocardial damage (Chen et al., 2020; Zhang et al., 2018, 2024a, 2025). However, despite growing recognition of its relevance to vascular aging, the precise spatiotemporal regulation of SIRT1-Nrf2 signaling during endothelial senescence, particularly in relation to membrane-bound receptor complexes, remains poorly defined.

Extracellular bioactive molecules, including polypeptides and proteins, typically initiate cellular responses by engaging transmembrane receptors and activating intracellular signaling cascades that govern diverse cellular functions. Among these receptors, CD44, a broadly expressed transmembrane glycoprotein, is markedly elevated in senescent vascular endothelial cells. Previous work has identified CD44 as a senescence-associated adhesion molecule that enhances monocyte recruitment to senescent endothelium, thereby implicating this receptor in the amplification of vascular inflammation during aging (Mun & Boo, 2010). A substantial body of evidence further indicates that CD44 modulates key cellular processes, including cell cycle progression, proliferation, and apoptosis, via its regulation of redox balance, inflammatory signaling, oxidative stress, and extracellular matrix remodeling (Zhao et al., 2007). These functions establish CD44 as a central mediator of endothelial senescence and a promising therapeutic target for anti-aging interventions. Given its dual role as both a senescence biomarker and functional regulator, CD44 may function as a membrane receptor linking extracellular peptide signals to intracellular anti-aging pathways. This putative signaling interface between bioactive peptides and CD44-mediated signaling represents a previously uncharacterized axis with significant potential for therapeutic innovation in age-related vascular decline.

This study identified AL-VI10, a novel peptide isolated from amphibian skin, as a potent modulator of vascular aging in D-galactose-induced models. Pharmacological and mechanistic analyses revealed that AL-VI10 suppressed endothelial senescence through CD44-mediated modulation of the SIRT1-Nrf2 signaling axis. These findings define a receptor-linked mechanism through which an extracellular peptide engages intracellular longevity pathways. Collectively, these findings establish AL-VI10 as a promising, low-cost candidate for vascular rejuvenation and reveal a previously unrecognized signaling axis with potential translational relevance for age-related cardiovascular disease.

MATERIALS AND METHODS

Screening of cDNA-encoded peptide AL-VI10 from *Amolops loloensis* skin transcriptome

The cDNA sequence encoding the AL-VI10 peptide was obtained from a previously constructed skin cDNA library of *A. loloensis*, as reported earlier (Wang et al., 2021). Briefly, recombinant clones containing inserts exceeding 300 bp were randomly selected and sequenced using an Applied Biosystems DNA sequencer (ABI 3730xl, USA) for identification of peptide-encoding transcripts.

Peptide synthesis and structural prediction

Synthetic AL-VI10, fluorescein isothiocyanate (FITC)-labeled AL-VI10, and a scrambled control peptide were commercially synthesized by Bioyears Biotechnology (China), with a purity greater than 95%. The mature peptide sequence was “VIPFVVSVVT”. Structure modeling was performed as

described in prior studies (Sun et al., 2023).

Hemolytic and cytotoxic assays of AL-VI10

The hemolytic activity of AL-VI10 was assessed using mouse erythrocytes, as described previously (Wang et al., 2025). Mouse erythrocytes were treated with AL-VI10, and hemoglobin release was quantified by measuring absorbance at 540 nm. A 0.5% (v/v) Triton X-100 solution was used as the positive control. Hemolytic activity was calculated using the formula:

$$[(A_{sample}) \times 100]/A_{TritonX\text{-}100} \quad (1)$$

Cytotoxicity was evaluated *in vitro* using a Calcein/PI Cell Viability/Cytotoxicity Assay Kit (C2015S; Beyotime, China), following the manufacturer's protocols. Live and dead cells were distinguished and analyzed by confocal laser scanning fluorescence microscopy (SpinSR10; Olympus, Japan).

Direct free radical scavenging activity assay of AL-VI10

Direct free radical scavenging activity of AL-VI10 was determined against two free radicals, 2,2-diphenyl-1-picrylhydrazyl (DPPH) and 2,2'-azinobis (3-ethylbenzothiazoline-6-sulfonic acid) ($ABTS^+$) (Sigma-Aldrich, USA), according to the kit instructions. $ABTS^+$ and DPPH radical scavenging rates (%) were calculated as:

$$\left[(A_{blank} - A_{sample}) \times 100\right]/A_{blank} \quad (2)$$

D-galactose-induced aging model and tissue preparation for hematoxylin and eosin (H&E) staining

Male C57BL/6 mice (6 weeks old) were obtained from Nuo Shun Biotechnology Co., Ltd (China). All animal procedures were performed in accordance with the guidelines approved by the Animal Ethics Committee of Kunming Medical University (kmmu20240245). Mice were housed under standard conditions with *ad libitum* access to food and water and were allowed to acclimatize for one week prior to experimental manipulation.

A vascular aging model was established through chronic subcutaneous injection of D-galactose (150 mg/kg) into the dorsal neck region for eight consecutive weeks. Mice were randomly assigned to three groups: young (vehicle only), aged (D-galactose 150 mg/kg), and aged+AL-VI10. Starting from week 5, the aged+AL-VI10 group received intravenous tail vein injections of AL-VI10 (100 ng/kg) once daily, while the other two groups received equivalent volumes of sterile saline. General health status and behavioral changes were monitored throughout the experimental period. Following model establishment, mice were anesthetized and thoracic aortas were carefully excised, embedded in optimal cutting temperature (OCT) compound (Sakura, USA), rapidly flash-frozen in liquid nitrogen, and stored at −80°C for subsequent histological analysis. Aortic cryosections (10 μm) were fixed in 4% paraformaldehyde for 15 min and washed three times with phosphate-buffered saline (PBS). Sections were then subjected to H&E staining with a commercial kit (Solarbio, China) according to the manufacturer's protocols. Aortic wall thickness was quantified with ImageJ (National Institutes of Health, USA).

Cell culture and establishment of hydrogen peroxide (H_2O_2)-induced senescent cell model

Human umbilical vein endothelial cells (HUVECs) were obtained from the Cell Bank of the Kunming Institute of Zoology, Chinese Academy of Sciences (KCB 2010233YJ). Cells were cultured in complete endothelial growth medium (Sciencell, USA) at 37°C in a humidified incubator with 5% CO_2. The medium was replaced every two days, with non-adherent cells removed and adherent cells retained for continued culture. To induce a senescent phenotype, confluent HUVECs were exposed to 200 μmol/L H_2O_2 for 24 h.

MTS assay for assessment of proliferative responses of senescent HUVECs to AL-VI10

Cell proliferation was evaluated by MTS assay after treatment of senescent HUVECs with AL-VI10 at 0.1, 1, and 10 nmol/L. Cells were seeded in 96-well plates at 5×10^3 cells/well and allowed to adhere before treatment. After the indicated intervention, 10 μL of MTS reagent (Promega, USA) was added to each well, and absorbance was measured at 490 nm. To examine the role of Nrf2 in the proliferative response and to determine the effect of AL-VI10 under Nrf2 inhibition, four groups were established: senescence control, senescence+AL-VI10 (10 nmol/L), senescence+ML385 (Nrf2 inhibitor, 10 μmol/L), and senescence+ML385 (10 μmol/L)+AL-VI10 (10 nmol/L). Cell proliferation was then quantified using the MTS method as described above.

Effects of AL-VI10 on cell scratch wounds in senescent HUVECs

HUVECs were seeded in 24-well plates (4×10^4 cells/well) and cultured to full confluence. A standardized scratch was created using a sterile 200 μL pipette tip. Following gentle washing with phosphate-buffered saline (PBS), the medium was replaced with serum-free endothelial culture medium. Cells were assigned to five groups: blank control (PBS), senescence (H_2O_2), and senescence+AL-VI10 (0.1, 1 and 10 nmol/L). For peptide intervention, cells were pre-incubated with AL-VI10 for 2 h prior to H_2O_2 exposure. Phase-contrast images of scratch wounds were captured at 0, 12, and 24 h using an inverted microscope. Wound areas were quantified using ImageJ, and wound closure percentage was calculated as:

$$[(\text{Scratch area at 0 h} - \text{Scratch area at 12 or 24 h})/\text{Scratch area at 0 h}] \times 100\% \quad (3)$$

Transwell assay for assessment of migration of senescent HUVECs after AL-VI10 treatment

Cell migration was evaluated with Transwell inserts (Corning, USA) containing 8 μm pores. Serum-free HUVEC suspensions (3×10^4 cells/well) were added to the upper chamber, and medium containing 12% fetal bovine serum (FBS) was added to the lower chamber. Experimental groups included a PBS control group, a senescence group treated with 200 μmol/L H_2O_2, and senescence+AL-VI10 groups pretreated with AL-VI10 at 0.1, 1, or 10 nmol/L for 2 h before H_2O_2 exposure. After incubation for 24 h, cells were fixed with 4% fixative, stained with 0.5% crystal violet, and imaged. Quantification was performed by dissolving the retained dye in 33% acetic acid and measuring absorbance at 570 nm.

Quantification of superoxide dismutase (SOD) and glutathione (GSH) levels

HUVECs were divided into five groups: blank control (PBS), senescent (H_2O_2), and H_2O_2+AL-VI10 (0.1, 1, and 10 nmol/L). After 24 h of treatment, cells were washed twice with ice-cold PBS, lysed on ice, and centrifuged at 12 000 ×*g* for 5 min at 4°C. The resulting supernatants were analyzed in quadruplicate using a commercial SOD assay kit (Beyotime, China). Samples were incubated at 37°C for 20 min, and

absorbance was measured at 450 nm to determine enzymatic activity.

Following mouse modeling, animals were anesthetized with 1% sodium pentobarbital and blood was collected via orbital puncture. After 2 h of clotting at room temperature, serum was obtained by centrifugation at 3 000 r/min for 15 min at 4°C. GSH concentrations were determined according to the manufacturer's instructions (Beyotime, China), with absorbance measured at 405 nm using a microplate reader.

Senescence-associated β-galactosidase (SA-β-gal) staining

Cells were divided into five groups: control (PBS), senescence (H_2O_2), and H_2O_2+AL-VI10 (0.1, 1, and 10 nmol/L). After treatment, staining was performed according to the manufacturer's protocols (Beyotime, China). Briefly, cells were washed twice with PBS, fixed with β-galactosidase fixative solution (1 mL/well) for 15 min, and washed three times with PBS. Freshly prepared staining solution was then applied, followed by overnight incubation at 37°C in a CO_2-free dark environment. Images were acquired using bright-field microscopy, and the senescence-positive rate was calculated as:

$$\text{(Number of blue-stained cells/Total number of cells)} \times 100\% \quad (4)$$

Detection of intracellular reactive oxygen species (ROS)

Intracellular ROS levels were assessed using a commercial detection kit according to the manufacturer's protocols (Beyotime, China). HUVECs were seeded into 35 mm confocal dishes (2×10^4 cells/well) and assigned to five groups: blank control (PBS), senescence (200 μmol/L H_2O_2), and H_2O_2+AL-VI10 (0.1, 1, and 10 nmol/L). After cell adhesion, AL-VI10 was administered for 2 h, followed by H_2O_2 treatment in all groups except the control group. Cells were then incubated with ROS-sensitive fluorescent probes for 25 min at 37°C in the dark and counterstained with Hoechst for 5 min. After three washes with serum-free medium, cells were imaged using super-resolution confocal microscopy.

Enzyme-linked immunosorbent assay (ELISA) and western blot analysis

Aortic tissue was dissected and rinsed with pre-cooled PBS to remove residual blood. After weighing, tissue samples were pulverized in liquid nitrogen and homogenized in PBS by ultrasonication to achieve complete cell lysis. Homogenates were centrifuged at 5 000 ×*g* for 20 min at 4°C, and supernatants were collected for measurement of interleukin-10 (IL-10) and interleukin-6 (IL-6) with commercial ELISA kits (NeoBioscience, China) according to the manufacturer's recommendations.

HUVECs were lysed in pre-cooled RIPA lysis buffer containing phenylmethylsulfonyl fluoride (PMSF; Solarbio, China) and centrifuged at 14 000 ×*g* for 20 min at 4°C. Supernatants were collected, and protein concentrations were determined before electrophoresis. Equal amounts of protein (30 μg per lane) were resolved by 8%–12% sodium dodecyl sulfate-polyacrylamide gel electrophoresis (SDS-PAGE) and transferred onto polyvinylidene fluoride (PVDF) membranes (Millipore, USA). After blocking with 5% skim milk (Solarbio, China) for 2 h at 20°C, membranes were incubated overnight at 4°C with the following primary antibodies: GAPDH (1:6 000; Proteintech, China), LaminB1 (1:2 000; Proteintech, China), p53 (1:6 000; Proteintech, China), p21 (1:2 000; Proteintech, China), p62 (1:1 000; CST, USA), LC3 (1:1 000; CST, USA), SIRT1 (1:1 000; CST, USA), CD44 (1:1 000; Proteintech, China), eNOS (1:1 000; BD Biosciences, USA), Nrf2 (1:1 000; Proteintech, China; 1:1 000; CST, USA), and MMP1 (1:1 000; Proteintech, China). Following three washes in Tris-buffered saline with Tween 20 (TBST), horseradish peroxidase (HRP)-conjugated secondary antibodies were applied for 1 h at 37°C. Protein bands were visualized using an enhanced chemiluminescence detection system (Biosharp, China) and analyzed using ImageJ.

Immunofluorescence

HUVECs were cultured on coverslips placed in plates, washed with PBS, and fixed with 4% paraformaldehyde. After blocking with 10% goat serum, cells were incubated overnight at 4°C with primary antibodies against SIRT1 (1:100; CST, USA) and Nrf2 (1:100; Proteintech, China). Following three PBS washes, cells were treated with FITC-conjugated secondary antibody (1:200; Proteintech, China) for 1 h and counterstained with 4',6-diamidino-2-phenylindole (DAPI; Sigma-Aldrich, USA). Samples were mounted and visualized under a fluorescence microscope, and images were analyzed using ImageJ. PBS instead of primary antibody served as the negative control for evaluation of nonspecific binding.

Molecular docking of AL-VI10 with the CD44 receptor

The three-dimensional (3D) structure of the CD44 receptor (PDB ID: 4PZ4) was retrieved from the Protein Data Bank (http://www.rcsb.org/pdb/). After removing redundant components, such as water molecules and small ligands, the structure was converted into PDBQT format using MGLTools v.1.5.7 (http://mgltools.scripps.edu). The AL-VI10 peptide structure was constructed in ChemDraw (https://www.cambridgesoft.com) and similarly processed into PDBQT format. Molecular docking was performed using AutoDock Vina v.1.1.2 (Oleg & Arthur, 2010) with the docking grid set to encompass the entire protein. The highest-scoring conformation (affinity=−6.8 kcal/mol) was selected for further analysis.

Lentiviral transduction and CD44 knockdown in HUVECs

Lentiviral vectors encoding either non-targeting control shRNA (LV-shRNA NC) or CD44-targeting shRNA (LV-shCD44) were obtained from Hanbio Biotechnology (China). The control siRNA sequence was TTCTCCGAACGTGTCACGTAA, and the CD44-targeting siRNA sequence was GCTGACCTCTG CAAGGCTTTCAATA. The corresponding shRNA sequences were as follows: Control shRNA: GATCCGAGCCTG GCGCAGATCGATTTGAATTTCAAGAGAATTCAAATCGATC TGCGCCAGGCTCTTTTTTG (top strand); AATTCAAAAA AGAGCCTGGCGCAGATCGATTTGAATTCTCTTGAAATTCA AATCGATCTGCGCCAGGCTCG (bottom strand). CD44-targeting shRNA: GATCCGCTGACCTCTGCAAGGCTTTC AATATTCAAGAGATATTGAAAGCCTTGCAGAGGTCAGCTT TTTTG (top strand); AATTCAAAAAAGCTGACCTCTGCAA GGCTTTCAATATCTCTTGAATATTGAAAGCCTTGCAGAGG TCAGCG (bottom strand).

HUVECs were seeded into 6-well plates and transduced with lentiviral vectors at a multiplicity of infection (MOI) of 30 in the presence of 4 μg/mL polybrene. After 72 h, puromycin selection was initiated to establish stable cell lines. Transduction efficiency was verified by western blot analysis and quantitative real-time polymerase chain reaction.

Reverse transcription-quantitative real-time polymerase chain reaction (RT-qPCR)

HUVECs transduced with lentiviral constructs (CD44-NC or

CD44-shRNA) were used for CD44 mRNA expression analysis. Total RNA was extracted using an Evo M-MLV RT-qPCR kit (Accurate biology, China) following the manufacturer's protocols. RNA concentration and purity were measured using a microspectrophotometer. Quantification of CD44 mRNA was performed on the LightCycler 480 SYBR PCR system, with GAPDH serving as the internal reference. Each group was analyzed in triplicate, and all experiments were independently repeated three times. Primer sequences were as follows: GAPDH (forward: ACCCACTCCTCCACCTTTG; reverse: CTCTTGTGCTCTTGCTGGG) and CD44 (forward: CTGCCGCTTTGCAGGTGTA; reverse: CATTGTGGGCAAG GTGCTATT). All primers were synthesized by Sangon Biotech (China).

Statistical analysis

All statistical analyses were performed using GraphPad Prism v.9 (GraphPad Software, USA). Data are expressed as mean±standard deviation (SD). Significant differences between groups were determined by Student's *t*-test or one-way analysis of variance (ANOVA), as appropriate. $P<0.05$ was considered statistically significant.

RESULTS

Structure characterization and biocompatibility assessment of AL-VI10

A novel bioactive peptide, designated AL-VI10, was identified from the skin secretions transcriptome of *A. loloensis* collected in Yuxi, Yunnan. The precursor contained 57 amino acid residues encoded by a 242 bp cDNA sequence, with a mature peptide amino acid sequence of "VIPFVVSVVT" (Figure 1A). Database searches using the NCBI (https://blast.ncbi.nlm.nih.gov/Blast.cgi) protein repository confirmed the absence of homologous sequences (data not shown), indicating that AL-VI10 represents a previously unreported novel bioactive peptide. The nomenclature AL-VI10 reflects its origin (AL, *A. loloensis*), the first two amino acids of the mature sequence (VI), and the total length of the peptide (10 residues).

Sequence and structural analyses revealed that AL-VI10 displayed the canonical organization of amphibian bioactive peptide precursors, including an N-terminal signal peptide, a central acidic fragment, and a C-terminal mature peptide. Nigrocin-6V1 was used as a reference peptide to support nomenclature assignment, delineation of the acidic region from the mature peptide sequence, and identification of the corresponding proteolytic cleavage sites (Figure 1B, C). Consistent with established proteolytic processing mechanisms for bioactive peptide maturation, the consensus recognition motif "KR" (lysine-arginine dipeptide) served as the proteolytic cleavage site. Post-translational cleavage at this KR site released the mature peptide and generated the final bioactive sequence VIPFVVSVVT. Mass spectrometric analysis yielded a molecular weight of 1 059.29 Da, and the predicted tertiary conformation together with the linear amino acid sequence is presented in Figure 1D, E.

To evaluate the biosafety profile of AL-VI10, cytotoxicity and hemolysis assays were conducted. Hemolytic potential was assessed using murine erythrocytes, with 0.9% NaCl used as a negative control (NC). Across all tested concentrations, AL-VI10 induced negligible hemoglobin release, indicating an absence of detectable erythrocyte lysis (Figure 1F). In parallel, cytotoxicity was further examined in HUVECs by calcein/propidium iodide (PI) dual staining. Cells treated with AL-VI10 (0.1, 1 and 10 nmol/L) displayed minimal PI-positive staining, comparable to untreated controls, whereas exposure to 10% DMSO caused marked PI uptake and substantial cell loss (Figure 1G). These data demonstrated that AL-VI10 produced neither cytotoxicity nor hemolysis within the tested concentration range, supporting its excellent biocompatibility. Antioxidant activity of AL-VI10 was further investigated using $ABTS^+$ and DPPH free radical scavenging assays. In both systems, AL-VI10 exhibited pronounced free radical scavenging activity. In the DPPH assay, AL-VI10 demonstrated dose-dependent antioxidant activity, with marked efficacy at different concentrations relative to the control group (Figure 1H). In the $ABTS^+$ assay, AL-VI10 exhibited robust radical neutralization across all tested concentrations (Figure 1I).

Together, these findings establish AL-VI10 as a structurally distinct and biologically safe peptide with potent antioxidant properties. Its favorable toxicity profile and radical-scavenging efficacy highlight its potential as a promising therapeutic candidate for further functional investigation.

AL-VI10 ameliorates vascular aging in a D-galactose-induced murine model

D-Galactose is a well-established inducer of acute aging, capable of promoting sustained oxidative stress, chronic inflammation, and apoptosis in vascular tissues (Wang et al., 2020). In this study, D-galactose was administered subcutaneously to induce vascular aging (Figure 2A), and the therapeutic efficacy of AL-VI10 was explored. Structural and functional deterioration of large arteries, characterized by medial thickening, luminal dilation, and extracellular matrix (ECM) remodeling, is a hallmark of vascular aging and frequently associated with excessive collagen deposition and disruption of smooth muscle cell architecture (Greenwald, 2007). No overt adverse effects, such as weight loss or abnormal behavioral manifestations, were observed following AL-VI10 administration. Histological analysis by H&E staining revealed pronounced age-associated vascular injury in D-galactose-treated mice, including thickening of the aortic medial layer and irregular alignment of vascular smooth muscle cells. Notably, AL-VI10 treatment markedly alleviated these pathological alterations and restored a more regular vascular architecture that more closely resembled the young phenotype (Figure 2B, C), indicating suppression of aging-associated vascular remodeling. To further define the molecular basis of this remodeling process, matrix metalloproteinase-1 (MMP1), a key enzyme involved in the degradation of collagen and other ECM components (Wang et al., 2023), was examined. Western blot analysis demonstrated a substantial up-regulation of MMP1 in aged aortic tissue, whereas AL-VI10 intervention substantially reduced this increase (Figure 2D, F), consistent with preservation of matrix integrity.

To validate the induction of vascular aging at the molecular level, the expression of canonical senescence markers, including tumor suppressor protein p53 and cyclin-dependent kinase inhibitor p21 (Afifi et al., 2023), was assessed. D-galactose-treated mice exhibited significant up-regulation of both markers in aortic tissue, confirming successful model establishment (Supplementary Figure S1). Notably, AL-VI10 (100 ng/kg) administration resulted in a marked reduction in p53 and p21 protein levels, as determined by western blot analysis (Figure 2D, G, H), indicating suppression of

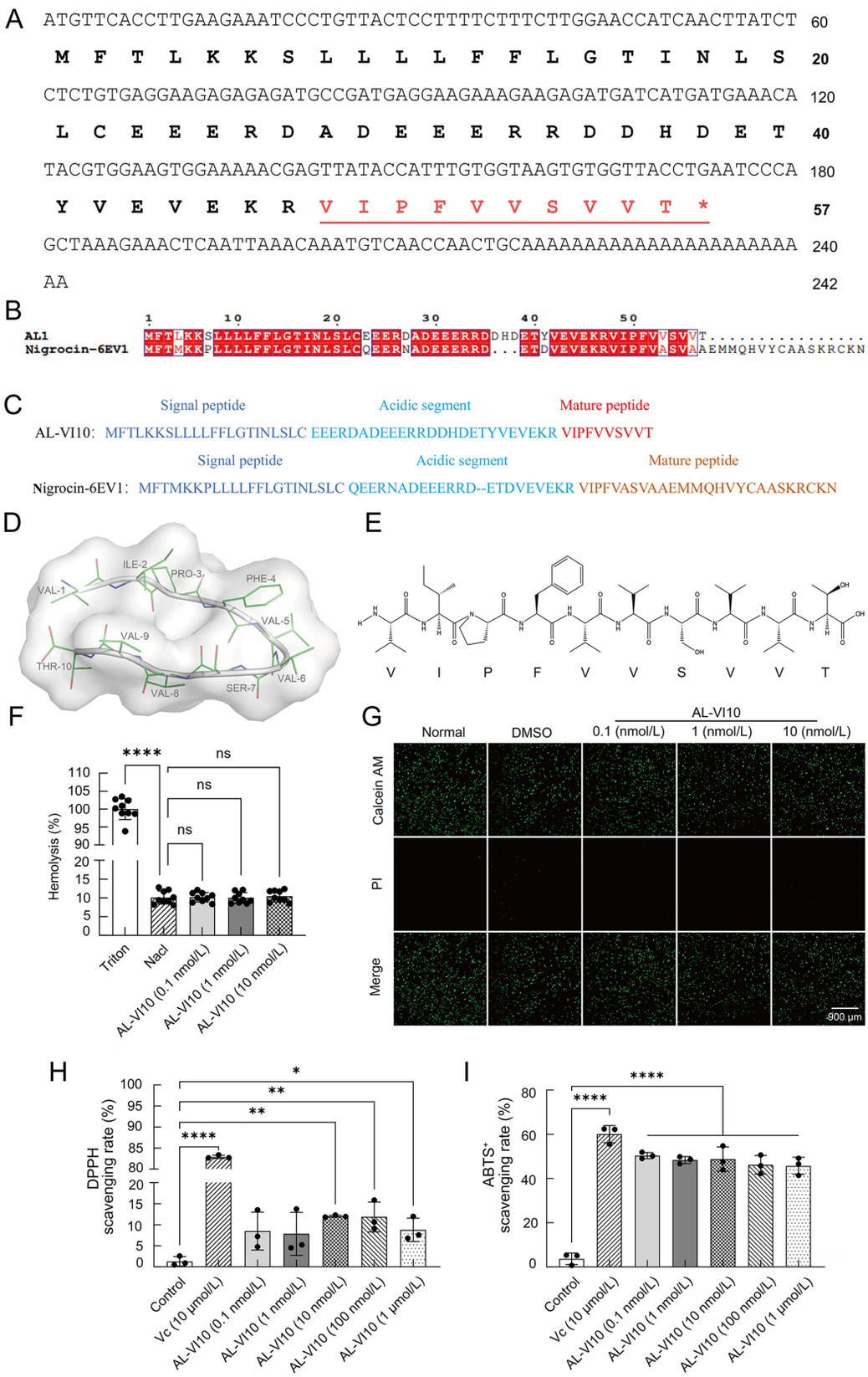

Figure 1 Structural characterization and biocompatibility assessment of AL-VI10

A: Precursor sequence of AL-VI10, which contained 57 amino acid residues encoded by a 242 bp cDNA sequence. Red sequence indicates the mature peptide region. B, C: Amino acid sequence of the AL-VI10 precursor peptide. Blue sequence indicates signal peptide of AL-VI10; red sequence indicates mature peptide. D, E: Predicted tertiary structure and linear amino acid sequence of AL-VI10. F: Hemolytic activity of AL-VI10 at different concentrations in erythrocytes from male KM mice (n=9). G: Cytotoxicity assessment of AL-VI10 in HUVECs. Representative confocal fluorescence images are shown for HUVECs treated with 10% DMSO or AL-VI10. Dead cells are shown in red, and viable cells are shown in green. Scale bar: 900 μm. H, I: Free radical scavenging activity of AL-VI10 against DPPH and $ABTS^+$ at all tested concentrations (n=3). All data are expressed as mean±SD. ns: Not significant; *: P<0.05; **: P<0.01; ****: P<0.0001.

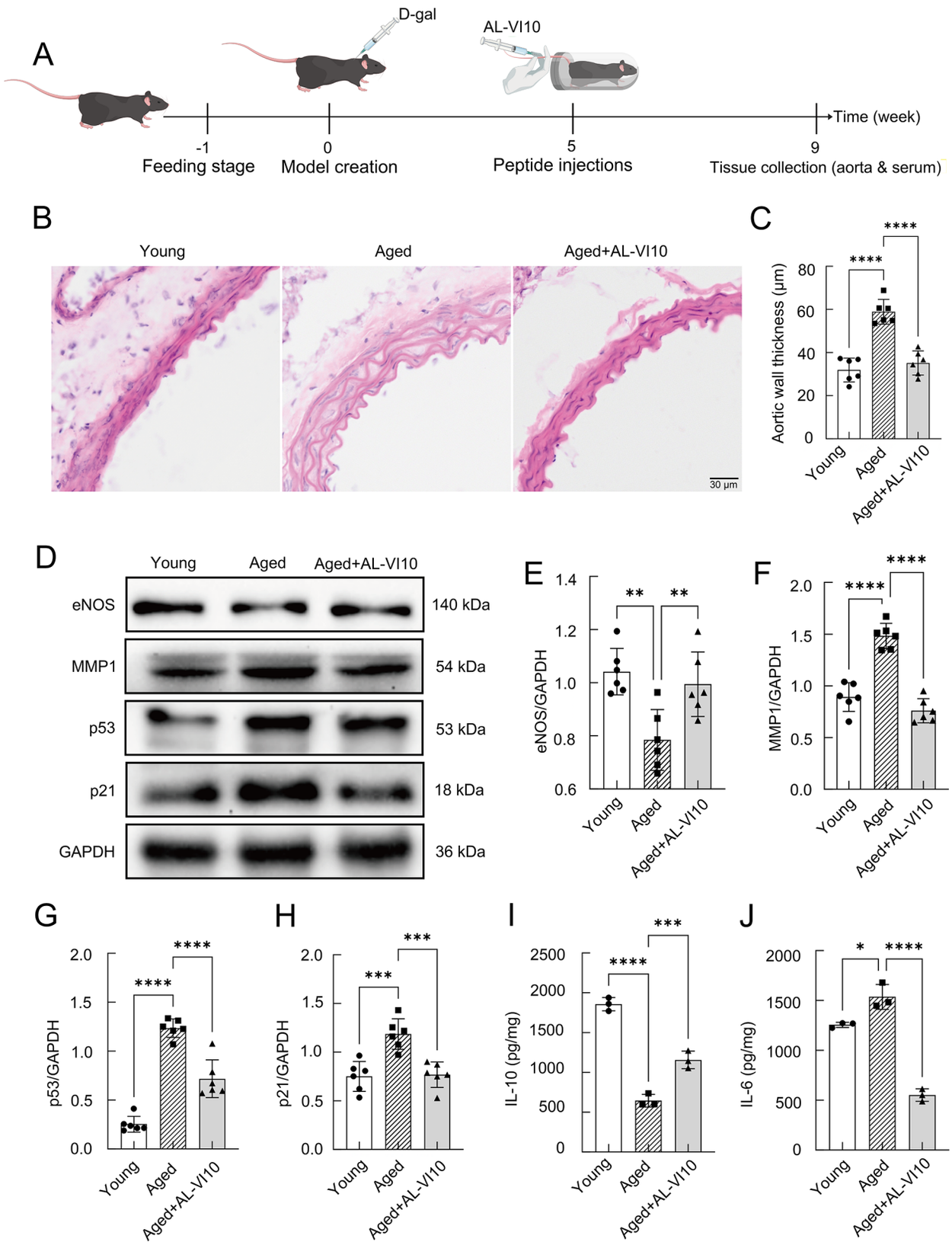

Figure 2 AL-VI10 ameliorates vascular aging in the D-galactose-induced murine model

A: Schematic showing AL-VI10 administration schedule in the D-galactose-induced mouse model of aging. B, C: H&E staining of aortic remodeling in mice and quantification of aortic wall thickness following AL-VI10 treatment (n=6). Scale bar: 30 μm. D: Western blot analysis of eNOS, MMP1, p53, and p21 in aortic tissue. E–H: Quantification of eNOS, MMP1, p53, and p21 protein levels in aortic tissue following AL-VI10 treatment (n=6). I, J: ELISA-based quantification of IL-10 and IL-6 levels in aortic tissue following AL-VI10 treatment (n=3). All data are expressed as mean±SD. *: P<0.05; **: P<0.01; ***: P<0.001; ****: P<0.0001.

senescence signaling and highlighting the therapeutic potential of AL-VI10 in vascular aging.

Chronic inflammation is a defining feature of D-galactose-induced aging (Wang et al., 2020). To assess the

immunoregulatory effects of AL-VI10, IL-10 and IL-6 levels were quantified in aortic tissue. Aged mice exhibited a pronounced reduction in IL-10 expression alongside a marked increase in IL-6. Administration of AL-VI10 reversed these changes, significantly elevating IL-10 while suppressing IL-6, as determined by ELISA (Figure 2I, J), indicating a shift toward an anti-inflammatory vascular microenvironment. Taken together, these findings demonstrate that AL-VI10 mitigates vascular aging-associated injury by suppressing inflammation and limiting ECM degradation, supporting further development of this peptide as a multifunctional therapeutic candidate for vascular aging.

AL-VI10 attenuates senescence in H_2O_2-induced senescent HUVECs

The vascular endothelium functions as a dynamic interface between circulating blood and the vessel wall, maintaining vascular homeostasis. Endothelial cell senescence is a critical driver of vascular aging and contributes to the pathogenesis of cardiovascular disease (Jia et al., 2019). To evaluate the anti-senescence potential of AL-VI10 on endothelial cells, an *in vitro* model of oxidative stress-induced senescence was established by exposing HUVECs to H_2O_2 (Supplementary Figure S2). Cellular senescence was assessed using SA-β-gal staining, alongside expression analyses of the canonical senescence markers p53 and p21. H_2O_2 exposure resulted in a marked increase in SA-β-gal-positive cells, characterized by prominent blue staining, indicating successful induction of senescence. Treatment with AL-VI10 effectively attenuated this senescence-associated enhancement, as evidenced by the reduced percentage of SA-β-gal-positive cells (Figure 3A, B). Western blot analysis further confirmed that H_2O_2 induced substantial up-regulation of p53 and p21 in senescent HUVECs. Consistently, AL-VI10 administration markedly reversed these alterations, demonstrating its potential to counteract endothelial cell senescence at the molecular level (Figure 3C, E, F).

These results collectively indicate that AL-VI10 effectively alleviates H_2O_2-induced endothelial cell senescence and may hold therapeutic potential for preserving vascular function under pro-aging conditions.

AL-VI10 improves functional capacity in senescent endothelial cells

In addition to endothelial cell senescence, vascular aging is characterized by progressive endothelial dysfunction, a central event in the pathogenesis of diverse cardiovascular disorders. Endothelial nitric oxide synthase (eNOS) serves as a critical regulator of vascular tone and is a key indicator of endothelial functional integrity during vascular aging. eNOS protein abundance was markedly reduced in both aged aortic tissue (Figure 2D, E) and senescent HUVECs (Figure 3C, D), indicating impaired nitric oxide-related endothelial activity. AL-VI10 treatment substantially reversed this decline in eNOS expression, consistent with improvement of endothelial functional status.

To further assess the effects of AL-VI10 on functional recovery of senescent endothelial cells, cell proliferation and migration were examined by MTS, scratch-wound, and Transwell assays. H_2O_2-induced senescence markedly impaired endothelial migratory capacity, as evidenced by reduced Transwell passage and delayed wound closure. Treatment with AL-VI10 significantly alleviated these defects, enhancing Transwell migration (Figure 3G, J) and accelerating wound closure in a concentration-dependent manner, with significant improvement observed at all tested concentrations (Figure 3H, K). These results indicate that AL-VI10 effectively restores motility in senescent endothelial cells. Proliferative capacity was further evaluated by MTS assay. H_2O_2 exposure significantly reduced cell viability, whereas AL-VI10 treatment for 24 h produced a dose-dependent increase in metabolic activity (Figure 3I), indicating recovery of proliferative potential.

Collectively, these findings indicate that AL-VI10 not only mitigates endothelial cell senescence but also improves key aspects of vascular endothelial function.

AL-VI10 reduces ROS accumulation and enhances antioxidant activity

To elucidate the antioxidant capacity of AL-VI10 *in vivo*, serum levels of GSH, a key systemic antioxidant, were assessed in D-galactose-treated mice. Aging resulted in a marked reduction in GSH concentration, whereas AL-VI10 intervention significantly restored this decline (Figure 4A). Oxidative stress is a central driver of endothelial senescence, primarily mediated by excessive accumulation of ROS. As such, suppression of ROS represents a promising therapeutic strategy for the prevention of endothelial senescence (Ke et al., 2018). To assess the antioxidant potential of AL-VI10 *in vitro*, intracellular ROS levels were quantified in H_2O_2-induced senescent HUVECs with a fluorescent probe-based detection assay. Exposure to H_2O_2 caused a pronounced increase in ROS accumulation. Subsequent treatment with AL-VI10 reduced intracellular ROS in a concentration-dependent manner, with the most pronounced effect observed at 10 nmol/L (Figure 4B, C). Antioxidant capacity of AL-VI10 was further assessed by measurement of SOD activity in HUVECs. Results indicated that SOD activity was markedly diminished in H_2O_2-induced senescent HUVECs, whereas AL-VI10 treatment progressively restored enzymatic activity across the tested concentration range (Figure 4D). These findings suggest that AL-VI10 alleviates oxidative stress through dual antioxidant actions, namely enhancement of endogenous antioxidant defense, reflected by increased GSH and SOD, and direct suppression of intracellular ROS accumulation in senescent endothelial cells.

AL-VI10 enhances autophagic activity in aged vasculature and senescent endothelial cells

Autophagy plays a fundamental role in cellular quality control by facilitating the removal of dysfunctional cellular components, with accumulating evidence demonstrating that autophagy can effectively delay aging and maintain cellular homeostasis (Torisu et al., 2016). During autophagy, p62 interacts with LC3 on the inner membrane of the autophagosome and facilitates selective cargo degradation. Accordingly, p62 abundance, together with the LC3-II/LC3-I ratio, serves as an indicator of autophagic activity (Du et al., 2024; Zeng et al., 2022). Our data revealed significant hallmarks of autophagic impairment in aged aortic tissue, characterized by a reduced LC3-II/LC3-I ratio and elevated expression of p62. AL-VI10 treatment reversed these alterations, increasing the LC3-II/LC3-I ratio and suppressing p62 protein levels (Figure 4E–G), indicative of enhanced autophagic flux. Similarly, H_2O_2-induced senescent HUVECs displayed a decline in autophagic activity, as evidenced by reduced LC3II levels and elevated p62 expression. AL-VI10 administration exhibited remarkable effects on autophagy regulation, with a marked decline in p62 levels and a marked increase in LC3II expression (Figure 4H–J). These findings

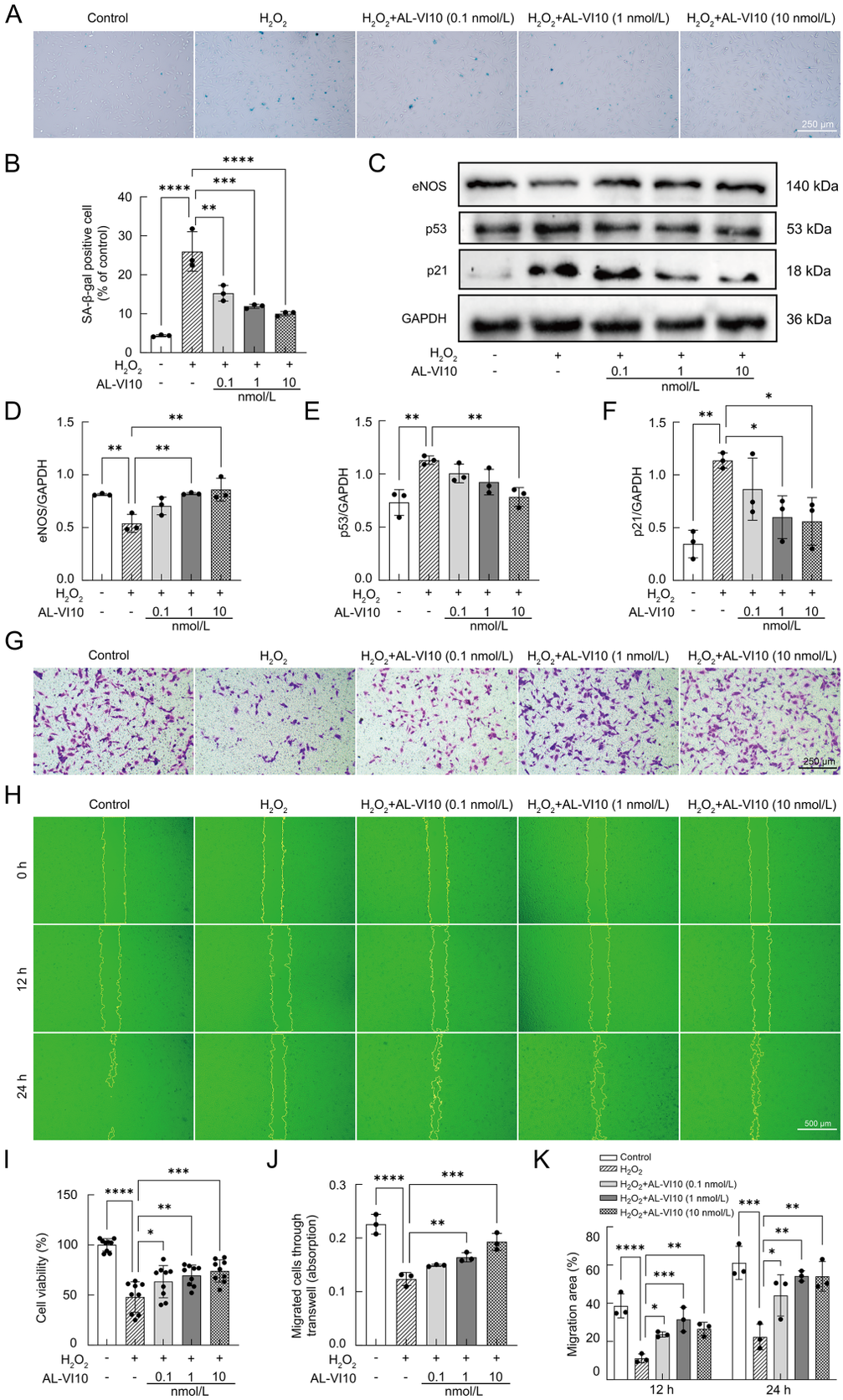

Figure 3 AL-VI10 attenuates senescence and restores functional capacity in H_2O_2-induced senescent HUVECs

HUVECs were treated with different concentrations of AL-VI10. A, B: Staining and quantification of SA-β-gal-positive cells in senescent HUVECs (*n*=3). Blue indicates SA-β-gal-positive cells. Scale bar: 250 μm. C: Western blot analysis of eNOS, p53, and p21 in senescent HUVECs. D–F: Quantification of eNOS, p53, and p21 protein levels in senescent HUVECs (*n*=3). G: Representative images of Transwell migration in senescent HUVECs. Scale bar: 250 μm. H: Cell scratch-wound assay at 0, 12, and 24 h in senescent HUVECs. Scale bar: 500 μm. I: MTS assay of proliferative activity of senescent HUVECs (*n*=9). J: Quantification of Transwell migration in senescent HUVECs (*n*=3). K: Quantification of scratch-wound healing in senescent HUVECs (*n*=3). All data are expressed as mean±SD. *: P<0.05; **: P<0.01; ***: P<0.001; ****: P<0.0001.

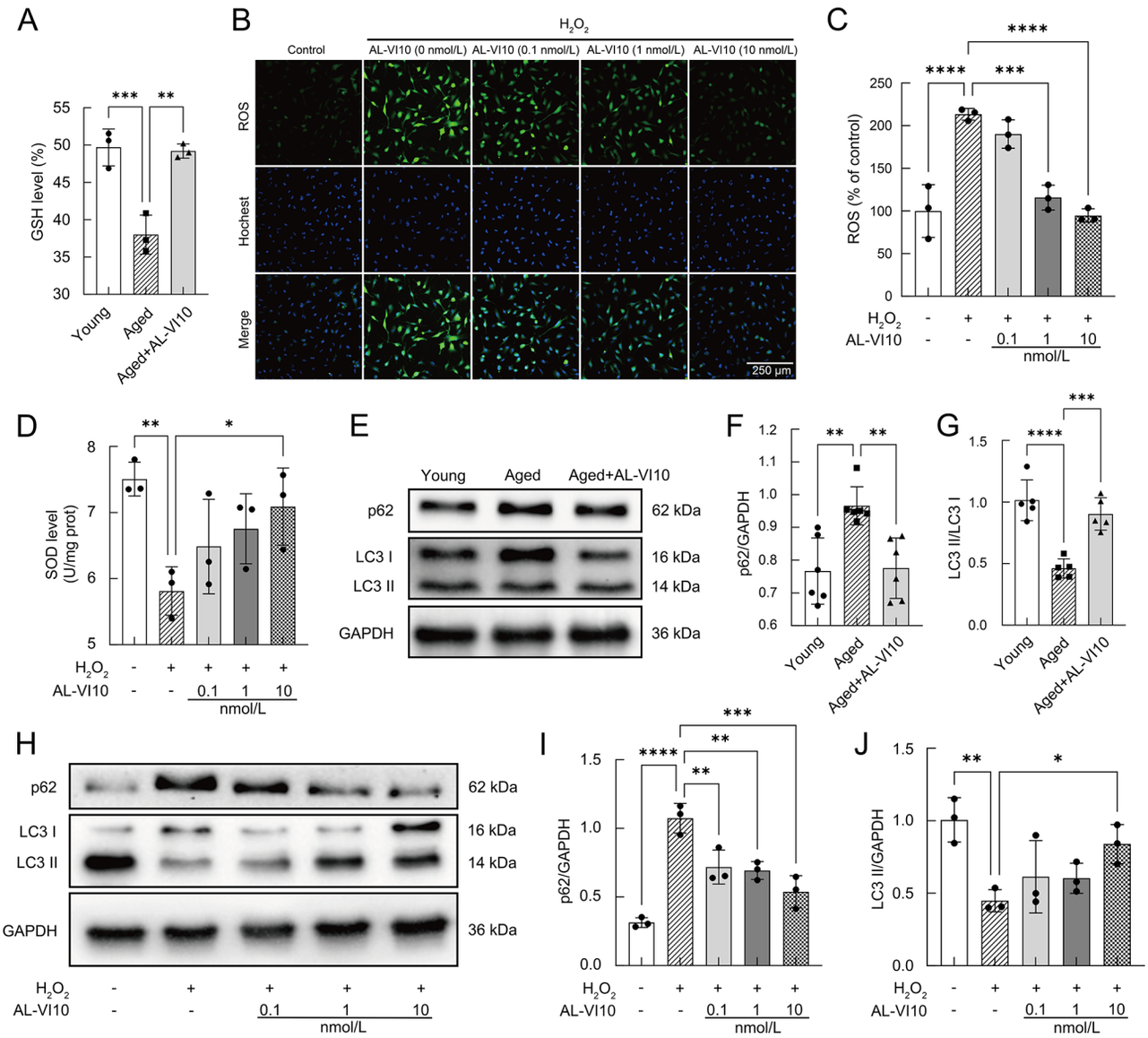

Figure 4 AL-VI10 attenuates oxidative stress, enhances antioxidant activity, and promotes autophagy

A: Serum GSH levels in mice following AL-VI10 treatment (n=3). B, C: Representative fluorescence images and quantification of intracellular ROS levels in HUVECs treated with different concentrations of AL-VI10 (n=3). Scale bar: 250 μm. D: SOD activity in HUVECs treated with different concentrations of AL-VI10 (n=3). E–G: Western blot analysis and quantification of p62 and LC3 protein levels in aged aortic tissue following AL-VI10 treatment (n=6). H–J: Western blot analysis and quantification of p62 and LC3 protein levels in senescent HUVECs following AL-VI10 treatment (n=3). All data are expressed as mean±SD. *: P<0.05; **: P<0.01; ***: P<0.001; ****: P<0.0001.

suggest that AL-VI10 restores impaired autophagy in both vascular tissue and senescent endothelial cells. By reactivating autophagic clearance mechanisms, AL-VI10 may contribute to the preservation of cellular homeostasis and delay vascular aging, underscoring its potential as a therapeutic modulator of autophagy in age-related vascular pathologies.

SIRT1 is required for AL-VI10-mediated suppression of vascular aging and endothelial senescence

SIRT1, a NAD^+-dependent deacetylase, is widely recognized as a key regulator of vascular longevity, exerting protective effects against oxidative stress, inflammation, and endothelial dysfunction. To determine whether SIRT1 mediates the anti-aging actions of AL-VI10, protein expression was first examined in aging vascular tissues. Western blot analysis revealed that SIRT1 levels were decreased in aging aortas, while AL-VI10 administration significantly restored SIRT1 expression (Figure 5A, C). A similar decline in SIRT1 expression was also observed in H_2O_2-induced senescent endothelial cells, with AL-VI10 treatment at varying concentrations, particularly 10 nmol/L, shown to markedly reverse this decline (Figure 5B, D). Based on these findings, 10 nmol/L was selected as the optimal concentration for subsequent experiments. Immunofluorescence analysis further confirmed that AL-VI10 treatment enhanced SIRT1 expression in HUVECs (Figure 5E, F).

The functional contribution of SIRT1 to the anti-senescence activity of AL-VI10 was then examined by pharmacological inhibition with EX527 (10 μmol/L), a selective SIRT1 inhibitor, in senescent HUVECs. Notably, inhibition of SIRT1 increased p53 and p21 protein levels relative to the AL-VI10-treated group. However, when AL-VI10 and EX527 were administered together, AL-VI10 significantly counteracted the effect of EX527 and reduced p53 and p21 expression (Figure 5G, I, J). These findings suggest that AL-VI10 suppresses endothelial

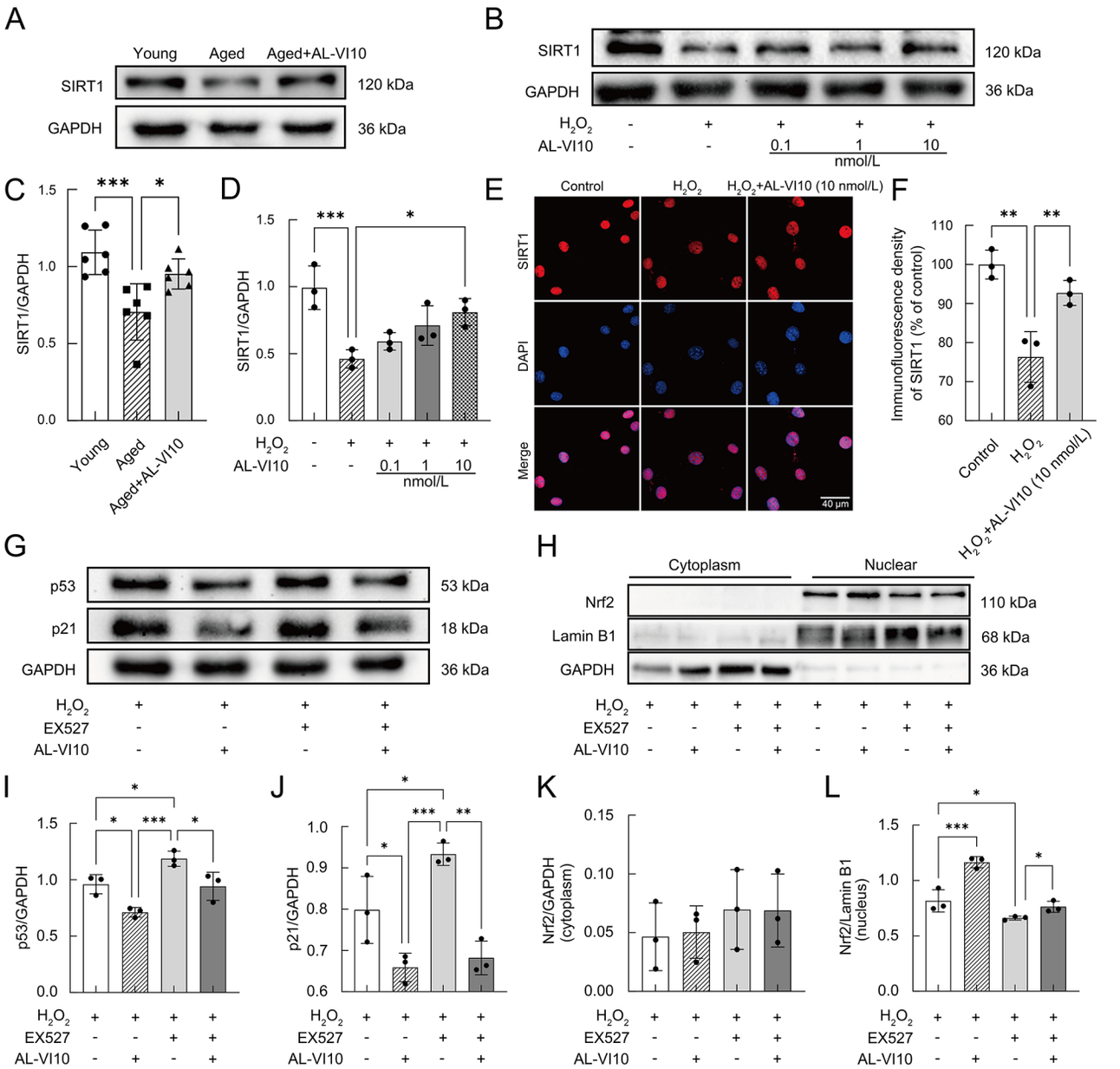

Figure 5 SIRT1 is required for AL-VI10-mediated attenuation of vascular aging and endothelial senescence

A: Western blot analysis of SIRT1 in aged mouse aortas following AL-VI10 treatment. B: Western blot analysis of SIRT1 in senescent HUVECs following AL-VI10 treatment. C, D: Quantification of SIRT1 protein levels in aged mouse aortas (n=6) and senescent HUVECs (n=3) following AL-VI10 treatment. E, F: Immunofluorescence staining and quantification of SIRT1 expression in senescent HUVECs following treatment with 10 nmol/L AL-VI10 (n=3). Scale bar: 40 μm. G: Western blot analysis of p53 and p21 in senescent HUVECs after SIRT1 inhibition with EX527 in the presence or absence of AL-VI10. H: Western blot analysis of cytoplasmic and nuclear Nrf2 in senescent HUVECs after SIRT1 inhibition with EX527 in the presence or absence of AL-VI10. I, J: Quantification of p53 and p21 protein levels in senescent HUVECs following treatment with EX527 in the presence or absence of AL-VI10 (n=3). K, L: Quantification of cytoplasmic and nuclear Nrf2 protein levels in senescent HUVECs following treatment with EX527 in the presence or absence of AL-VI10 (n=3). All data are expressed as mean±SD. *: P<0.05; **: P<0.01; ***: P<0.001.

senescence, at least in part, through activation of SIRT1, thereby providing new mechanistic insight into vascular aging and identifying potential therapeutic targets for age-related vascular disease.

Nrf2 is necessary for AL-VI10 and SIRT1-mediated protection against endothelial senescence

To elucidate downstream targets involved in the anti-senescence effects of AL-VI10, the role of Nrf2 was investigated. Under physiological conditions, Nrf2 is sequestered in the cytoplasm in an inactive state. Upon activation, it translocates to the nucleus, where it binds antioxidant response elements and up-regulates the expression of antioxidant enzymes, thereby playing a key role in antioxidant defense (Singh et al., 2010). Western blot analysis revealed that Nrf2 expression was significantly reduced in D-galactose-induced aging aortas, whereas AL-VI10 treatment restored Nrf2 protein levels (Figure 6A, C). In senescent HUVECs, decreased Nrf2 expression was also observed, but AL-VI10 administration induced a marked elevation in nuclear Nrf2 levels, indicating enhanced transcriptional activation (Figure 6B, D, E). These findings were confirmed by immunofluorescence staining, which demonstrated increased nuclear localization of Nrf2 following AL-VI10 treatment (Figure 6G, H).

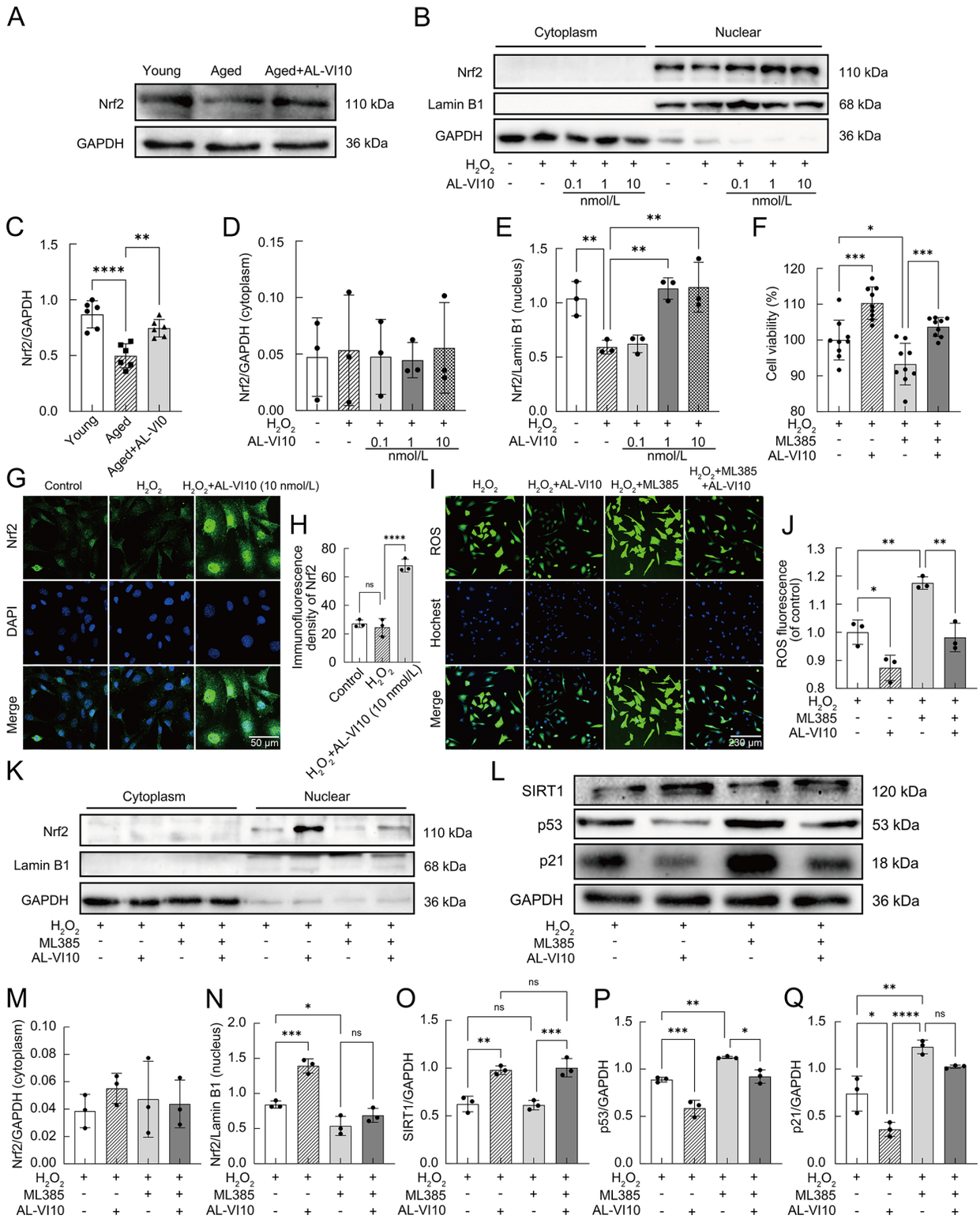

Figure 6 Nrf2 is essential for the anti-senescence effects of AL-VI10

A: Western blot analysis of Nrf2 in aged mouse aortas following AL-VI10 treatment. B: Western blot analysis of cytoplasmic and nuclear Nrf2 in senescent HUVECs following AL-VI10 administration. C–E: Quantification of Nrf2 protein expression in aged mouse aortas (*n*=6) and in the cytoplasmic and nuclear fractions of senescent HUVECs following AL-VI10 treatment (*n*=3). F: MTS assay of proliferative activity of senescent HUVECs after ML385 intervention in the presence or absence of AL-VI10 (*n*=9). G, H: Immunofluorescence staining and quantification of Nrf2 expression in senescent HUVECs following treatment with 10 nmol/L AL-VI10 (*n*=3). Scale bar: 50 μm. I, J: Representative immunofluorescence images and quantification of intracellular ROS levels in senescent HUVECs treated with ML385 in the presence or absence of AL-VI10 (*n*=3). Scale bar: 230 μm. K: Western blot analysis of cytoplasmic and nuclear Nrf2 in senescent HUVECs treated with ML385 in the presence or absence of AL-VI10. L: Western blot analysis of SIRT1, p53, and p21 in senescent HUVECs after ML385 treatment in the presence or absence of AL-VI10. M–Q: Quantification of cytoplasmic and nuclear Nrf2, together with SIRT1, p53, and p21 protein levels, in senescent HUVECs after ML385 treatment in the presence or absence of AL-VI10 (*n*=3). All data are expressed as mean±SD. ns: Not significant; *: $P<0.05$; **: $P<0.01$; ***: $P<0.001$; ****: $P<0.0001$.

To further determine whether SIRT1 activation contributes to Nrf2 nuclear translocation, senescent endothelial cells were treated with EX527. Pharmacological inhibition of SIRT1 attenuated AL-VI10-induced nuclear accumulation of Nrf2, suggesting that SIRT1 functions upstream of Nrf2 in this setting. Notably, AL-VI10 partially restored nuclear Nrf2 localization even under SIRT1 inhibition, suggesting that additional regulatory mechanisms may also contribute to this response (Figure 5H, K, L). To further establish the functional role of Nrf2, senescent HUVECs were treated with ML385, a specific Nrf2 inhibitor. Nrf2 inhibition impaired cell proliferation (Figure 6F) and increased intracellular ROS accumulation (Figure 6I, J). Western blot analysis confirmed marked suppression of Nrf2 expression following ML385 treatment (Figure 6K, M, N). Furthermore, inhibition of Nrf2 abolished the anti-senescence effects of AL-VI10, as indicated by increased expression of the senescence markers p53 and p21 (Figure 6L, P, Q). AL-VI10 administration counteracted these adverse effects, partially restoring redox balance and attenuating senescence-associated protein expression. Notably, Nrf2 inhibition did not alter SIRT1 expression (Figure 6L, O), further supporting the conclusion that Nrf2 functions downstream of SIRT1 in the AL-VI10-modulated anti-aging cascade.

These findings collectively demonstrate that Nrf2 activation is indispensable for AL-VI10-mediated attenuation of endothelial senescence and functions as a downstream effector of SIRT1 signaling. AL-VI10 thus exerts its protective actions through coordinated activation of the SIRT1-Nrf2 axis, promoting both the expression and nuclear translocation of Nrf2.

AL-VI10 attenuates endothelial senescence by targeting the membrane receptor CD44 in HUVECs

Transmembrane receptors play a fundamental role in transducing extracellular signals into intracellular responses (Yoshikawa, 2015). Among these, CD44, a single-pass type I transmembrane glycoprotein, has emerged as a crucial regulator in vascular aging and a potential molecular target for anti-aging interventions (Mun & Boo, 2010). Molecular docking simulations revealed that AL-VI10 specifically interacted with the extracellular domain of CD44 within the inner cavity region, stabilized by a network of hydrogen bonds and electrostatic forces (Figure 7A). Supporting this, fluorescence colocalization experiments demonstrated strong spatial overlap between FITC-labeled AL-VI10 and CD44 immunostaining outside the nuclear region of HUVECs (Figure 7B), indicating that CD44 serves as a membrane binding partner mediating AL-VI10 uptake and downstream signaling.

To functionally validate this interaction, a stable CD44-knockdown model was established in HUVECs using lentiviral infection. Efficient silencing was confirmed at both protein levels by western blot analysis (Figure 7C, E) and RT-qPCR (Figure 7H). Notably, CD44 silencing significantly down-regulated senescence-associated markers p53 and p21 (Figure 7C, F, G), demonstrating that CD44 knockdown effectively attenuates endothelial senescence.

To elucidate the mechanistic relationship between CD44 and AL-VI10, four experimental conditions were compared: NC, NC+AL-VI10, CD44-shRNA (CD44 knockdown), and CD44-shRNA+AL-VI10. Comparative analysis revealed that both the NC+AL-VI10 and CD44-shRNA groups showed significantly increased SIRT1 expression while down-regulating CD44 and p53 levels relative to the NC group, with more prominent effects observed in the CD44-shRNA group. Notably, in the CD44-shRNA+AL-VI10 group, although SIRT1 levels remained elevated and CD44 and p53 levels were suppressed compared to the NC group, no additional significant changes were detected compared to the CD44-shRNA group (Figure 7D, I–K). This suggests that the effects of the peptide are dependent on CD44 binding and cannot further modulate these molecular markers when CD44 expression is already ablated.

Taken together, these findings provide compelling evidence that AL-VI10 exerts its anti-senescence effects through specific interactions with the CD44 receptor, subsequently activating the intracellular SIRT1-Nrf2 signaling cascade. This mechanistic insight establishes CD44 as a critical mediator of AL-VI10-induced vascular rejuvenation and highlights its potential as a therapeutic entry point for interventions targeting aging-associated endothelial dysfunction.

DISCUSSION

The present study identified AL-VI10 as a novel amphibian-derived bioactive peptide with pronounced protective activity against vascular aging. In H_2O_2-induced senescent endothelial cells, AL-VI10 alleviated the senescent phenotype and restored key aspects of endothelial function. Mechanistic analyses further indicated that AL-VI10 engaged the membrane receptor CD44 and triggered activation of the SIRT1-Nrf2 signaling cascade. Together, these findings define a receptor-linked molecular mechanism underlying the anti-aging effects of AL-VI10 and support its potential as a therapeutic candidate for aging-associated vascular disorders.

Vascular aging involves a multifaceted cascade of pathophysiological events, including increased intima-medial thickness, disorganized vascular smooth muscle architecture, matrix metalloproteinase dysregulation, chronic inflammation, impaired autophagy, and accelerated endothelial senescence (Guan et al., 2024; Wang et al., 2024). These processes collectively drive vascular deterioration and promote development of aging-related vascular disease. In the present study, AL-VI10 reversed many hallmark features of this phenotype in the aging aorta, improving tissue architecture and reducing expression of senescence-associated markers. As the primary vascular cell population, endothelial cells play a pivotal role in vascular tone and homeostasis, and impaired endothelial structure and function represent major determinants of vascular aging, significantly influencing the initiation, progression, and clinical severity of age-related vascular pathologies (Augustin & Koh, 2024). Within this framework, AL-VI10 administration enhanced endothelial proliferation and migration, suppressed ROS accumulation, increased eNOS expression, and ameliorated premature cellular senescence, collectively indicating substantial recovery of endothelial integrity and function.

While prior studies have identified several classes of bioactive peptides, including endogenous vasoactive peptides and mussel-derived bioactive peptides, as modulators of aging-related processes (Chen et al., 2022; Zhou et al., 2014), the present study represents the first characterization of anti-vascular aging efficacy mediated by a small bioactive peptide derived from amphibian skin. AL-VI10 also exhibited several favorable pharmacological properties, including low molecular weight, minimal amino acid residues, no apparent requirement for post-translational modification, and compatibility with high-

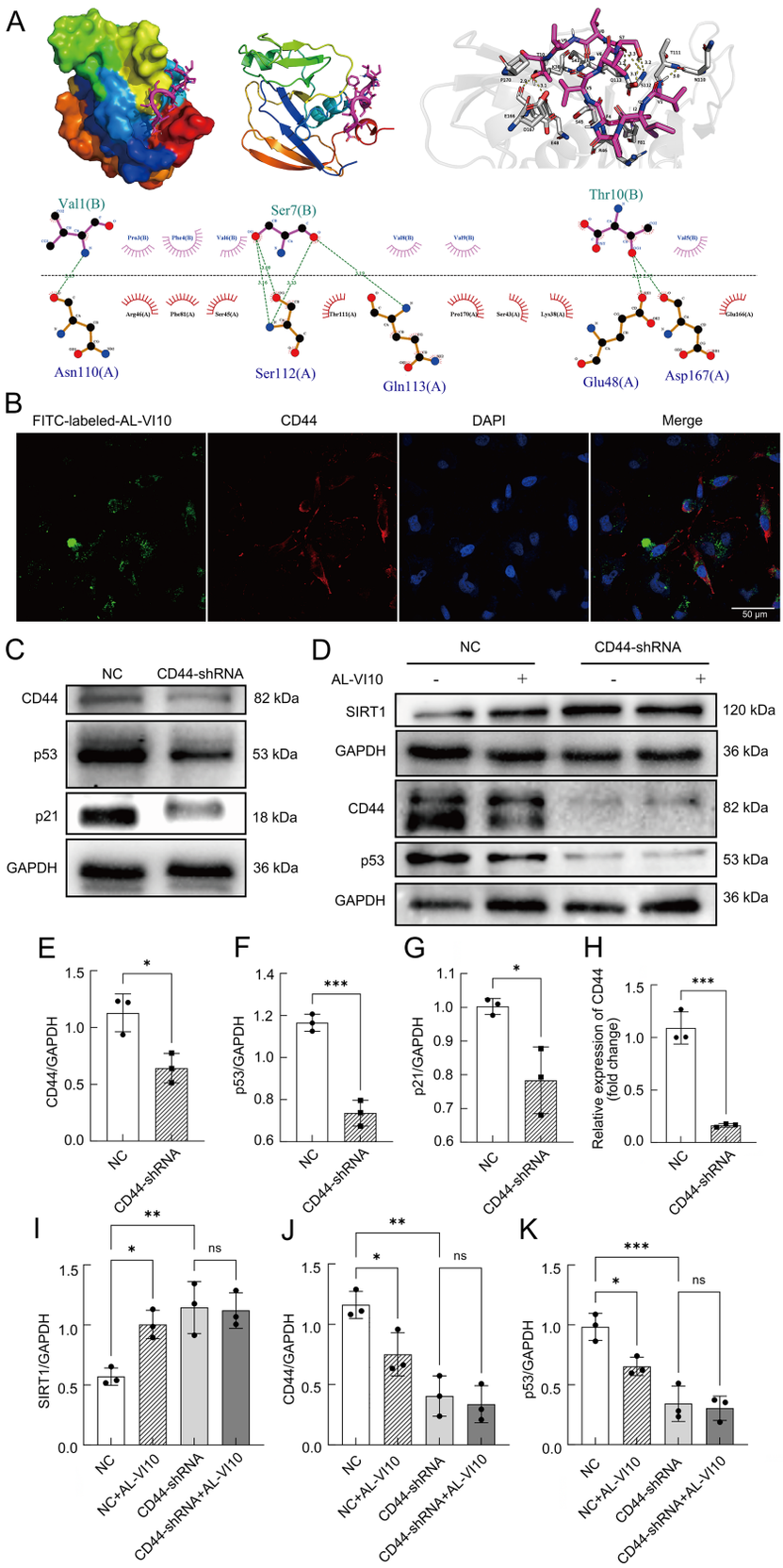

Figure 7 AL-VI10 attenuates vascular endothelial senescence by targeting the membrane receptor CD44 in HUVECs

A: Molecular docking model showing the interaction between AL-VI10 and CD44. B: Immunofluorescence colocalization of CD44 and AL-VI10 in HUVECs. Green indicates FITC-labeled AL-VI10, red indicates CD44 staining, and blue indicates nuclei stained with DAPI. Scale bar: 50 μm. C: Western blot analysis of CD44, p53, and p21 following CD44 knockdown in HUVECs. D: Western blot analysis of SIRT1, CD44, and p53 following CD44 knockdown in HUVECs in the presence or absence of AL-VI10. E–G: Quantification of CD44, p53, and p21 protein levels following CD44 knockdown in HUVECs (*n*=3). H: RT-qPCR analysis confirming CD44 knockdown efficiency (*n*=3). I–K: Quantification of SIRT1, CD44, and p53 protein levels in CD44-knockdown HUVECs in the presence or absence of AL-VI10 (*n*=3). All data are expressed as mean±SD. ns: Not significant; *: *P*<0.05; **: *P*<0.01; ***: *P*<0.001; ****: *P*<0.0001.

yield, low-cost solid-phase synthesis. These attributes, together with the robust biological activity observed in the current study, establish AL-VI10 as a promising candidate for further development as a therapeutic agent against vascular aging.

SIRT1, a member of the sirtuin family, is a well-established regulator of longevity (Kumar & Kumar, 2022). Previous studies have demonstrated that targeted overexpression of SIRT1 in vascular endothelial cells protects against aging-associated dysfunction and cellular senescence, offering a potential therapeutic approach for age-related vascular pathologies (Campagna et al., 2024). In this study, AL-VI10 significantly up-regulated SIRT1 expression in both aged aortic tissue and senescent endothelial cells. Pharmacological inhibition of SIRT1 attenuated the anti-senescence effects of AL-VI10, indicating that its protective actions are, at least in part, SIRT1-dependent. Nevertheless, partial restoration of these effects under SIRT1 blockade suggests additional regulatory mechanisms may also contribute to AL-VI10 activity.

Nrf2 is a master regulator of antioxidant defense and plays a central role in longevity by preserving redox homeostasis and restricting intracellular ROS accumulation. Age-associated impairment of vascular Nrf2 signaling exacerbates oxidative stress and increases susceptibility of aged vessels to cellular damage (Wu et al., 2022; Xu et al., 2024). The present study demonstrated that AL-VI10 activated Nrf2 in both aged aortic tissue and senescent endothelial cells and promoted nuclear translocation, consistent with induction of antioxidant transcriptional programs. Moreover, pharmacological inhibition of SIRT1 markedly reduced nuclear Nrf2 expression, while inhibition of Nrf2 significantly abolished the anti-senescence effects of AL-VI10, as indicated by up-regulated expression of aging markers, increased ROS accumulation, and impaired cell proliferation. These observations align with previous evidence implicating Nrf2 as a central mediator of cellular defense against oxidative stress during aging (Chen, 2021; Csiszar et al., 2007). Although AL-VI10 promoted nuclear translocation of Nrf2, the exact molecular mechanism by which this peptide activates the antioxidant pathway remains to be clarified. Notably, blockade of Nrf2 had no impact on SIRT1 expression, reinforcing the view that Nrf2 functions downstream of SIRT1. Together, these results support a model in which AL-VI10 attenuates endothelial senescence through SIRT1-driven activation of the Nrf2 signaling axis, highlighting Nrf2 as a key effector in AL-VI10-mediated vascular protection.

Emerging evidence has underscored the importance of peptide-receptor interactions in orchestrating cellular processes (Ru et al., 2025). For example, OA-RD17 administration has been shown to enhance keratinocyte proliferation and migration via Toll-like receptor 4 (TLR4)-mediated activation of the MAPK signaling pathway (Li et al., 2023). Similarly, Andersonin-W1 has been shown to bind to TLR4 in the extracellular region, modulating NF-κB signaling and demonstrating remarkable efficacy in diabetic wound healing (Li et al., 2024). Given the molecular weight of AL-VI10 (1 059.29 Da), efficient membrane penetration and direct intracellular action are likely limited, raising the possibility that this peptide exerts its biological effects through a cell-surface receptor. Prior studies using knockout mouse models have demonstrated that loss of CD44 is correlated with improved vascular function and attenuation of age-related pathological changes, while elevated CD44 expression in aged vasculature is associated with decreased vascular function and increased cardiovascular disease risk (Lowe & Raj, 2014). Furthermore, Zhang et al. (2023) demonstrated that CD44 modulates autophagic activity, implicating this receptor in the decline of autophagy associated with endothelial aging. Consistent with these observations, the present study detected marked up-regulation of CD44 in senescent HUVECs, prompting evaluation of CD44 as a potential target of AL-VI10. Molecular docking and immunofluorescence colocalization analyses supported interaction between AL-VI10 and CD44 in the extracellular region. Functional studies further showed that CD44 knockdown in HUVECs up-regulated SIRT1 and down-regulated senescence markers p53 and p21. Strikingly, AL-VI10 failed to induce additional changes in SIRT1 expression or senescence markers in CD44-knockdown cells, strongly indicating that the biological activity of AL-VI10 depended on CD44. While the molecular events linking CD44 engagement to SIRT1 up-regulation remain to be resolved, several intermediary mechanisms may be involved, including altered NAD^+ availability, crosstalk with other membrane receptors, or modulation of upstream kinases controlling SIRT1 activity, all of which warrant further investigation. Given the established role of the SIRT1-Nrf2 axis in the anti-senescence activity of AL-VI10, these findings support a model in which AL-VI10 engages CD44 at the cell surface and initiates intracellular signaling that ultimately activates the SIRT1-Nrf2 pathway, thereby attenuating endothelial cell senescence.

Several study limitations should be acknowledged. First, this study relied primarily on induced senescence models to assess the efficacy of AL-VI10 and to investigate the underlying mechanisms. Although these models recapitulated core features of vascular aging, the effects of AL-VI10 in naturally aged systems, including aged animal models, remain to be established. Second, although molecular docking and functional analyses supported CD44 as the primary binding partner of AL-VI10, the binding specificity and structural basis of this interaction have not been fully delineated. Detailed structural studies will be essential to clarify how AL-VI10 selectively engages CD44 and modulates its downstream signaling.

CONCLUSIONS

This study provides the first evidence that an amphibian-derived bioactive peptide can effectively mitigate vascular aging. Mechanistically, AL-VI10 acted through membrane-bound CD44 to activate SIRT1-Nrf2 signaling, thereby attenuating oxidative stress and suppressing cellular senescence. These findings expand current understanding of how exogenous small peptides can modulate aging-associated vascular dysfunction. In addition to strong biological efficacy, the favorable safety profile of AL-VI10, including absence of detectable cytotoxicity and hemolysis together with physicochemical stability, identifies this peptide as a promising candidate for therapeutic development in vascular aging and related pathologies.

SUPPLEMENTARY DATA

Supplementary data to this article can be found online.

COMPETING INTERESTS

The authors declare that they have no competing interests.

AUTHORS' CONTRIBUTIONS

X.W.Y. conceived the project. X.L., J.L., and B.L. contributed to data

curation, methodology, project administration, visualization, and writing of the original draft. Z.H.Q., G.R.Z., H.Y.G., Z.R.L., X.Y.H., Z.W., Y.S.L., X.Y.Z., L.T.W., and S.G.Y conducted the research and acquired the data. W.R.S., L.H., and Y.W. supervised the study. M.Y.L. and X.W.Y. reviewed and revised the manuscript. X.W.Y. and Y.W. acquired funding. All authors read and approved the final version of the manuscript.

ACKNOWLEDGMENTS

We thank all individuals who generously participated in this research. We also acknowledge the helpful comments provided by the reviewers and editors on this manuscript.

REFERENCES

Afifi MM, Crncec A, Cornwell JA, et al. 2023. Irreversible cell cycle exit associated with senescence is mediated by constitutive MYC degradation. *Cell Reports*, **42**(9): 113079.

Augustin HG, Koh GY. 2024. A systems view of the vascular endothelium in health and disease. *Cell*, **187**(18): 4833–4858.

Campagna R, Mazzanti L, Pompei V, et al. 2024. The multifaceted role of endothelial Sirt1 in vascular aging: an update. *Cells*, **13**(17): 1469.

Chen QM. 2021. Nrf2 for cardiac protection: pharmacological options against oxidative stress. *Trends in Pharmacological Sciences*, **42**(9): 729–744.

Chen Y, Qi YF, Lu WW. 2022. Endogenous vasoactive peptides and vascular aging-related diseases. *Oxidative Medicine and Cellular Longevity*, **2022**: 1534470.

Chen ZH, Yu J, Fu ML, et al. 2020. Dipeptidyl peptidase-4 inhibition improves endothelial senescence by activating AMPK/SIRT1/Nrf2 signaling pathway. *Biochemical Pharmacology*, **177**: 113951.

Csiszar A, Labinskyy N, Zhao XM, et al. 2007. Vascular superoxide and hydrogen peroxide production and oxidative stress resistance in two closely related rodent species with disparate longevity. *Aging Cell*, **6**(6): 783–797.

De La Torre BG, Albericio F. 2020. Peptide therapeutics 2.0. *Molecules*, **25**(10): 2293.

Deng CJ, Wang Y, Yang XW. 2026. Amphibian-derived peptides as novel therapeutics for skin wound healing: mechanisms, applications, and challenges. *Zoological Research*. DOI: 10.24272/j.issn.2095-8137.2026.076.

Donato AJ, Machin DR, Lesniewski LA. 2018. Mechanisms of dysfunction in the aging vasculature and role in age-related disease. *Circulation Research*, **123**(7): 825–848.

Du J, Liu W, Song YJ, et al. 2024. Activating autophagy promotes skin regeneration induced by mechanical stretch during tissue expansion. *Burns & Trauma*, **12**: tkad057.

Fu Z, Jiang JY, Jia QY. 2026. The self-assembling amphibian-derived peptide (RADA)4-FZ1 pioneers a novel therapeutic platform for diabetic skin wound management. *Chemical Engineering Journal*, **530**: 173231.

Greenwald SE. 2007. Ageing of the conduit arteries. *The Journal of Pathology*, **211**(2): 157–172.

Guan Q, Zhang Y, Wang ZK, et al. 2024. Skeletal phenotypes and molecular mechanisms in aging mice. *Zoological Research*, **45**(4): 724–746.

Jia GH, Aroor AR, Jia C, et al. 2019. Endothelial cell senescence in aging-related vascular dysfunction. *Biochimica et Biophysica Acta (BBA) - Molecular Basis of Disease*, **1865**(7): 1802–1809.

Jia QY, Fu Z, Li YS, et al. 2024. Hydrogel loaded with peptide-containing nanocomplexes: symphonic cooperation of photothermal antimicrobial nanoparticles and prohealing peptides for the treatment of infected wounds. *ACS Applied Materials & Interfaces*, **16**(11): 13422–13438.

Ke YL, Li D, Zhao MM, et al. 2018. Gut flora-dependent metabolite Trimethylamine-N-oxide accelerates endothelial cell senescence and vascular aging through oxidative stress. *Free Radical Biology and Medicine*, **116**: 88–100.

Kumar J, Kumar S. 2022. Sirtuin1 in vascular endothelial function, an overview. *Epigenetics*, **17**(9): 953–969.

Li C, Fu Z, Jin T, et al. 2023. A frog peptide provides new strategies for the intervention against skin wound healing. *Cellular & Molecular Biology Letters*, **28**(1): 61.

Li C, Xiong YX, Fu Z, et al. 2024. The direct binding of bioactive peptide Andersonin-W1 to TLR4 expedites the healing of diabetic skin wounds. *Cellular & Molecular Biology Letters*, **29**(1): 24.

Li YS, Jia QY, Liu NX, et al. 2025b. Peptide RL-QN15 regulates functions of epidermal stem cells to accelerate skin wound regeneration via the FZD8/β-Catenin axis. *Exploration*, 20240090

Lowe D, Raj K. 2014. Premature aging induced by radiation exhibits pro-atherosclerotic effects mediated by epigenetic activation of CD44 expression. *Aging Cell*, **13**(5): 900–910.

Lu HP, Chai JW, Xu ZJ, et al. 2024. Cath-KP, a novel peptide derived from frog skin, prevents oxidative stress damage in a Parkinson's disease model. *Zoological Research*, **45**(1): 108–124.

Mun GI, Boo YC. 2010. Identification of CD44 as a senescence-induced cell adhesion gene responsible for the enhanced monocyte recruitment to senescent endothelial cells. *American Journal of Physiology-Heart and Circulatory Physiology*, **298**(6): H2102–H2111.

Oleg T, Arthur JO. 2010. AutoDock Vina: improving the speed and accuracy of docking with a new scoring function, efficient optimization, and multithreading. *J Comput Chem*, **31**(2): 455–61.

Ru ZQ, Wu YT, Yang CY, et al. 2025. Ultra-short cyclic peptide $Cy_{RL\text{-}QN15}$ acts as a TLR4 antagonist to expedite oral ulcer healing. *Zoological Research*, **46**(5): 1187–1202.

Shen BY, Wang YL, Cheng JQ, et al. 2023. Pterostilbene alleviated NAFLD via AMPK/mTOR signaling pathways and autophagy by promoting Nrf2. *Phytomedicine*, **109**: 154561.

Singh S, Vrishni S, Singh BK, et al. 2010. Nrf2-ARE stress response mechanism: a control point in oxidative stress-mediated dysfunctions and chronic inflammatory diseases. *Free Radical Research*, **44**(11): 1267–1288.

Sun DD, Guo K, Liu NX, et al. 2023. Peptide RL-QN15 promotes wound healing of diabetic foot ulcers through p38 mitogen-activated protein kinase and smad3/miR-4482-3p/vascular endothelial growth factor B axis. *Burns & Trauma*, **11**: tkad035.

Tao LY, Lu XF, Fu ZJ, et al. 2023. Tong Sai granule improves AECOPD via regulation of MAPK-SIRT1-NF-κB pathway and cellular senescence alleviation. *Journal of Ethnopharmacology*, **314**: 116622.

Torisu K, Singh KK, Torisu T, et al. 2016. Intact endothelial autophagy is required to maintain vascular lipid homeostasis. *Aging Cell*, **15**(1): 187–191.

Wang LP, Chen QW, Zhuang SQ, et al. 2020. Effect of *Anoectochilus roxburghii* flavonoids extract on H_2O_2 - induced oxidative stress in LO2 cells and D-gal induced aging mice model. *Journal of Ethnopharmacology*, **254**: 112670.

Wang LT, Fu Z, Su YH, et al. 2025. Cyclic heptapeptide FZ1 acts as an integrin αvβ3 agonist to facilitate diabetic skin wound healing by enhancing angiogenesis. *Journal of Medicinal Chemistry*, **68**(18): 19503–19520.

Wang X, Jia JK, Wang Q, et al. 2024. *Myotis* bat STING attenuates aging-related inflammation in female mice. *Zoological Research*, **45**(5): 961–971.

Wang X, Shi WZ, Wang K, et al. 2023. Rationally designed nonapeptides with great skin photoprotective effect through producing type 1 collagen and blocking the mTOR pathway. *Journal of Medicinal Chemistry*, **66**(11): 7615–7628.

Wang Y, Feng Z, Yang MF, et al. 2021. Discovery of a novel short peptide with efficacy in accelerating the healing of skin wounds. *Pharmacological Research*, **163**: 105296.

Wei ZQ, Li XG, Zhou JY, et al. 2025. Inhibition of miRNA-365-2-5p targeting SIRT1 regulates functions of keratinocytes to enhance wound healing. *The FASEB Journal*, **39**(8): e70560.

Wu XY, Wei JJ, Yi Y, et al. 2022. Activation of Nrf2 signaling: a key molecular mechanism of protection against cardiovascular diseases by natural products. *Frontiers in Pharmacology*, **13**: 1057918.

Wu YT, Ru ZQ, Peng Y, et al. 2024. Peptide $Cy_{RL\text{-}QN15}$ accelerates hair regeneration in diabetic mice by binding to the Frizzled-7 receptor. *Zoological Research*, **45**(6): 1287–1299.

Xu LJ, An TT, Jia BH, et al. 2024. Histone deacetylase 3-specific inhibitor RGFP966 attenuates oxidative stress and inflammation after traumatic brain injury by activating the Nrf2 pathway. *Burns & Trauma*, **12**: tkad062.

Yoshikawa M. 2015. Bioactive peptides derived from natural proteins with respect to diversity of their receptors and physiological effects. *Peptides*, **72**: 208–225.

Zeng X, Zhang YD, Ma RY, et al. 2022. Activated Drp1 regulates p62-mediated autophagic flux and aggravates inflammation in cerebral ischemia-reperfusion via the ROS-RIP1/RIP3-exosome axis. *Military Medical Research*, **9**(1): 25.

Zhang B, Zhai MG, Li BY, et al. 2018. Honokiol ameliorates myocardial ischemia/reperfusion injury in type 1 diabetic rats by reducing oxidative stress and apoptosis through activating the SIRT1-Nrf2 signaling pathway. *Oxidative Medicine and Cellular Longevity*, **2018**(1): 3159801.

Zhang JC, Hu HQ, Zhu YT, et al. 2025. Bushen Jianpi Tiaoxue Decoction (BJTD) ameliorates oxidative stress and apoptosis induced by uterus ageing through activation of the SIRT1/NRF2 pathway. *Phytomedicine*, **136**: 156288.

Zhang L, Yang PC, Chen JX, et al. 2023. CD44 connects autophagy decline and ageing in the vascular endothelium. *Nature Communications*, **14**(1): 5524.

Zhang Y, Hei F, Xiao YJ, et al. 2024a. Acidic fibroblast growth factor inhibits reactive oxygen species-induced epithelial–mesenchymal transdifferentiation in vascular endothelial cells via the miR-155-5p/SIRT1/Nrf2/HO-1 pathway to promote wound healing in diabetic mice. *Burns & Trauma*, **12**: tkae010.

Zhang YX, Kang ZJ, Wang JJ, et al. 2024b. Peptide OM-LV20 promotes arteriogenesis induced by femoral artery ligature via the miR-29b-3p/VEGFA axis. *Atherosclerosis*, **391**: 117487.

Zhao L, Hall JA, Levenkova N, et al. 2007. CD44 regulates vascular gene expression in a proatherogenic environment. *Arteriosclerosis, Thrombosis, and Vascular Biology*, **27**(4): 886–892.

Zhou Y, Dong Y, Xu QG, et al. 2014. Mussel oligopeptides protect human fibroblasts from hydrogen peroxide (H_2O_2)-induced premature senescence. *Archives of Gerontology and Geriatrics*, **58**(2): 293–299.

Zhu YY, Zhao LM, Jia XY, et al. 2025. Amphibians as a source of bioactive antioxidant peptides: Emerging insights and therapeutic potential. *Zoological Research*, **46**(5): 1219–1243.